Comparative Analysis of Pseudo-Potential and Tight-Binding Band Structure Calculations with an Analytical Two-Band k·p Model: Conduction Band of Silicon

Viktor A. Sverdlov[a,b], Hans Kosina[a], Siegfried Selberherr[a]
[a]Institute for Microelectronics, TU Wien, 1040 Wien, Austria;
[b]V.A. Fock Institute of Physics, State University of St.Petersburg, 198904 St.Petersburg, Russia.

ABSTRACT

An analytical two-band **k·p** model for the conduction band of silicon is compared with the numerical nonlocal empirical pseudo-potential method and the $sp^3d^5s^*$ nearest-neighbor tight-binding model. The two-band **k·p** model gives results consistent with the empirical pseudo-potential method and describes the conduction band structure accurately. The tight-binding model overestimates the gap between the two lowest conduction bands at the valley minima, which results in an underestimation of the non-parabolicity effects. When shear strain is introduced, the two-band **k·p** model predicts an analytical expression for the strain-dependence of the band structure, which is in good agreement with results of pseudo-potential simulations.

Keywords: silicon band structure, **k·p** theory, tight-binding method, empirical pseudo-potential method.

1. INTRODUCTION

The **k·p** theory describes the band structure analytically. After the pioneering work by Luttinger and Kohn [1] the six-band **k·p** method has become widely used to model the valence band of cubic semiconductors. Usually the conduction band in silicon is approximated by three pairs of equivalent minima located near the *X*-points of the Brillouin zone. It is assumed that close to the minima the electron dispersion is parabolic and well described by the effective mass approximation.

A non-parabolic isotropic dispersion describes deviations in the density of states from the purely parabolic expression, which become important at higher electron energies. In ultra-thin body (UTB) FETs with (110) UTB orientation, however, a direction-dependent non-parabolicity must be introduced to explain the mobility behavior at high carrier concentrations [2]. Therefore, a more refined description of the conduction band minima beyond the usual single-band non-parabolic anisotropic approximation is needed.

Another reason to challenge this standard approximation is its inability to properly describe the band structure modification under shear stress. A recent experimental study [3] indicates that a shear distortion, which is inherent to [110] uniaxial stress used in the semiconductor industry to enhance the performance of n-MOSFETs, leads to a dependence of the transversal effective masses on stress. This conclusion is also supported by recent results of pseudo-potential band structure calculations [3,4]. Since the transversal mass determines the mobility in a FET with ultra-thin Si body, the electron mobility enhancement induced by [110] tensile stress in such FETs is solely due to a decrease of the conductivity mass in the stress direction [4-6]. Shear strain substantially modifies not only both transversal [4-7], but also the longitudinal [5,6] effective masses. Any dependence of the **k·p** effective masses on stress is neglected within the single-band description of the conduction band and can only be introduced phenomenologically. In order to describe the dependence of the effective mass on stress, a single-band description is not sufficient. Coupling to other bands has to be taken into account.

A 30 bands **k·p** theory was introduced recently [8]. Although universal, it cannot provide an explicit analytical solution for the energy dispersion. In this work we present an efficient two-band **k·p** theory. By comparing our results with predictions of the empirical pseudo-potential method we demonstrate that the theory accurately describes the stress induced band structure modification due to shear stress and allows to study the influence of the conduction band structure on transport properties of stressed Si.

Micro- and Nanoelectronics 2007, edited by Kamil A. Valiev, Alexander A. Orlikovsky,
Proc. of SPIE Vol. 7025, 70251I, (2008)
0277-786X/08/$18 · doi: 10.1117/12.802503

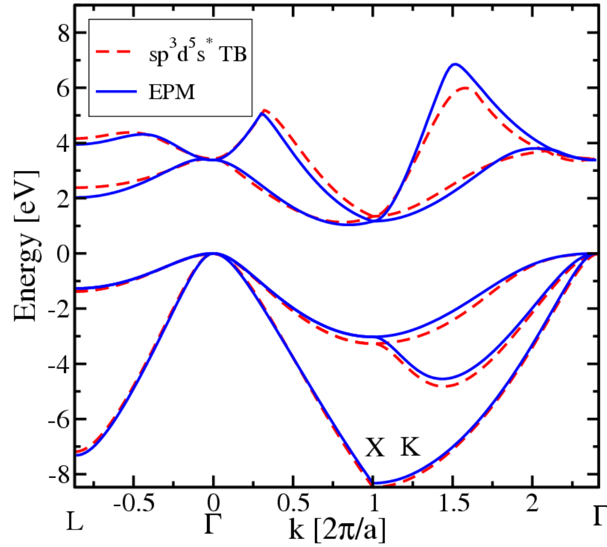

Fig. 1. Band structure of silicon from the EPM (solid lines) and from the $sp^3d^5s^*$ model (dashed lines).

2. EMPIRICAL NONLOCAL PSEUDO-POTENTIAL AND TIGHT-BINDING BAND STRUCTURE CALCULATIONS

We use the empirical nonlocal pseudo-potential method (EPM) for numerical band structure calculations. The parameters of the EPM method are adjusted in order to reproduce the measurable quantities of semiconductors related to the band structure: energy gap and effective masses. The method includes spin-orbit coupling. In our calculations of the silicon band structure we used the parameters from [9].

Recently, empirical tight-binding methods for band structure calculations became popular. Agreement between the band structures obtained from the EPM and the $sp^3d^5s^*$ model with the parameters from [10] is good as shown in Fig.1. However, the conduction band minimum in the $sp^3d^5s^*$ model is further away from the X point than in EPM, where the valley minimum is located at the distance $k_0 = 0.15\,(2\pi / a)$ from the X point. This leads to an almost two times higher

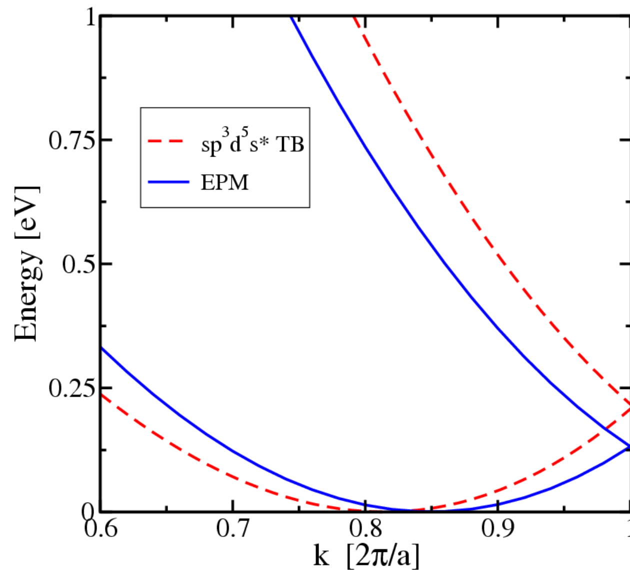

Fig. 2. Conduction bands close to the valley minimum. The EPM (solid lines) reproduces the band structure accurately.

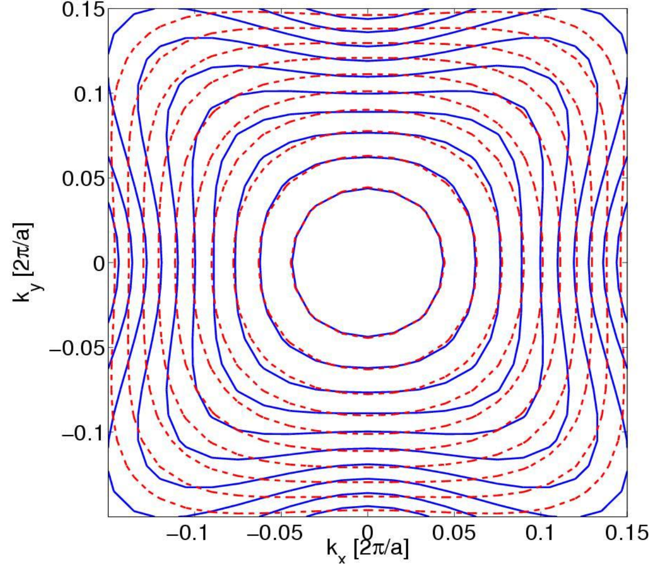

Fig. 3. Comparison of the k_x, k_y energy dispersion relations at the minimum position $k_z = k_0$ as obtained from EPM (solid lines) and the tight-binding method (dashed lines). The contour lines are spaced every 50 meV.

gap between the two lowest conduction bands at the valley minima (Fig.2) compared to Δ = 0.53 eV found from the EPM. The increase in the gap reduces the coupling between the conduction bands. Since the non-parabolicity of the lowest conduction band is determined by the coupling with other bands as shown in the next section, the higher gap predicted by the tight-binding method results in a substantially lower non-parabolicty of the band. It also results in a different shape of the constant energy lines in the k_x, k_y plane at $k_z = -k_0$. Fig.3 shows that the EPM gives a more pronounced band warping than the *sp^3d^5s** tight-binding model.

3. TWO-BAND K·P MODEL

We consider the valley pair along the [001] direction. Other valleys can be analyzed in a similar fashion. The band closest to the first conduction band Δ_1 (i=1) is the second conduction band $\Delta_{2'}$ (i=2). The two bands become degenerate exactly at the *X* points. Since the minimum of the conduction band is only k_0 away from the *X* point, the dispersion around the minimum is well described by degenerate perturbation theory which includes only these two bands. Diagonal elements of the Hamiltonian H_{ii} at the *X* point are:

$$H_{ii}(\mathbf{k}) = \frac{\hbar^2 k_z^2}{2m_l} + (-1)^i \frac{k_z p}{m_0} + \frac{\hbar^2 (k_x^2 + k_y^2)}{2m_t}, \qquad i = 1, 2 \tag{1}$$

where m_0 is the free electron mass, m_t is the transversal and m_l the longitudinal effective mass. The values of k_z are counted from the *X* point and are thus negative. The coupling between the two bands is described by the off-diagonal terms [7]:

$$H_{12}(\mathbf{k}) = \frac{\hbar^2 k_x k_y}{M}, \qquad \{2\}$$

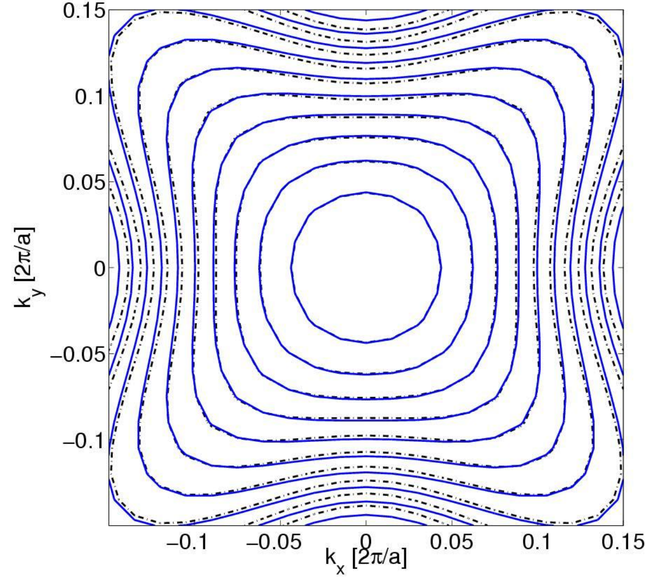

Fig. 4. Comparison of the dispersion relation (3) at the valley minimum (dashed-dotted lines) with the EPM results (solid lines). The distance between the equi-energy contour lines is 50 meV.

The parameter M^{-1} is obtained from the **k·p** perturbation theory:

$$\frac{1}{M} = \frac{2}{m_0^2} \sum_{l \neq 1,2} \frac{(p_y)_{l1}(p_x)_{2l}}{E_l - E_1} \ .$$

We use for M^{-1} the value computed by the EPM at the *X* point $M^{-1} = 0.8 m_t^{-1}$, where the numerical value is close (but not equal) to $M^{-1} \approx m_t^{-1} - m_0^{-1}$ reported in [7]. With degenerate perturbation theory we obtain the following dispersion relation for the lowest band:

$$E(\mathbf{k}) = \frac{\hbar^2 k_z^2}{2m_l} + \frac{\hbar^2 (k_x^2 + k_y^2)}{2m_t} - \sqrt{\left(\frac{k_z p}{m_0}\right)^2 + \left(\frac{\hbar^2 k_x k_y}{M}\right)^2} \ . \tag{3}$$

Expanding (3) around the minimum $k_z = k_0 = p m_l / m_0$ with respect to $q_z = k_z - k_0$, one obtains a simplified dispersion relation [11]:

$$E(\mathbf{k}) = \frac{\hbar^2 q_z^2}{2m_l} + \frac{\hbar^2 (k_x^2 + k_y^2)}{2m_t} - \frac{1}{\Delta}\left(\frac{\hbar^2 k_x k_y}{M}\right)^2 - \frac{\Delta}{4}, \tag{4}$$

where $\Delta = 2\frac{\hbar^2 k_0 p}{m_0} = 2\frac{\hbar^2 k_0^2}{m_l}$ is the gap between the Δ_1 and the $\Delta_{2'}$ conduction bands at $k_z = -k_0$. To estimate the value of the non-parabolicity parameter, we follow [11], Appendix B, and average out the angular dependence in (4). Assuming $\alpha E(\mathbf{k})$ to be small and recasting terms, one finally obtains:

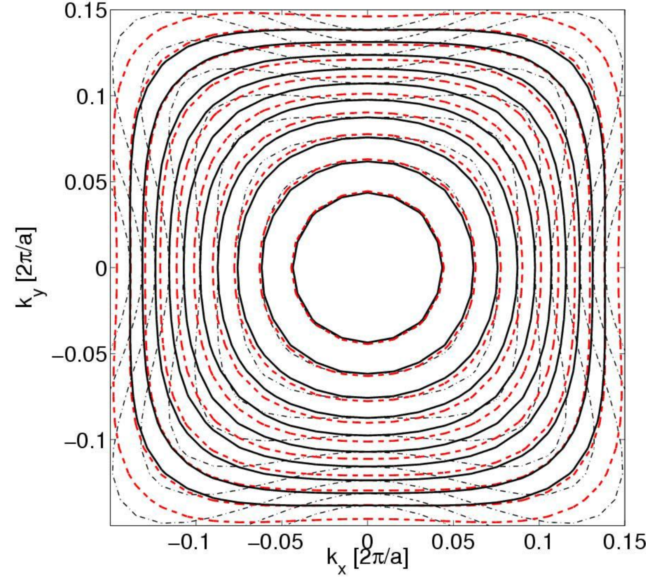

Fig. 5. Dispersion at the valley minimum obtained from the $sp^3d^5s^*$ model (dashed lines), from (3) with the correct EPM value Δ=0.53 eV (dotted-dashed lines), and from (3) with Δ=1.2 eV (solid lines). The distance between the equi-energy contour lines is 50 meV.

$$\frac{\hbar^2(k_x^2+k_y^2)}{2m_t} = E(\mathbf{k})\left(1+\alpha E(\mathbf{k})\right)$$

with [11]

$$\alpha = \frac{1}{2\Delta}\left(\frac{m_t}{M}\right)^2 \tag{5}$$

Substituting the parameter values for Si in (5), we estimate α = 0.6 eV^{-1}, which is close to the empirical value of α = 0.5 eV^{-1}.

In Fig.4 the analytical expression is compared to the numerical band structure obtained from the EPM at $k_z = -k_0$. Excellent agreement is found up to the energy 0.5 eV. Fig.4 displays a pronounced warping of the conduction band at higher energies. On the other hand, Fig.3 shows that the $sp^3d^5s^*$ model predicts less anisotropy (dashed contour lines). As indicated in Fig.2, the gap between the two lowest conduction bands predicted by the $sp^3d^5s^*$ model is nonrealistically large. This results in a smaller coupling between the bands. The solid contour lines shown in Fig.5 obtained from (3) with a nonrealistic value of Δ = 1.2 eV reproduce the results of the tight-binding model. This confirms the observation that the larger gap between the two bands at the valley minimum results in less anisotropy of the conduction band.

4. SHEAR STRAIN

Uniaxial stress along the [110] direction generates diagonal ε_{jj}, $j = x, y, z$ as well as off-diagonal ε_{xy} components of the strain tensor in the principal coordinate system. The diagonal components are added to the diagonal matrix elements (1) of the [001] valley [12]:

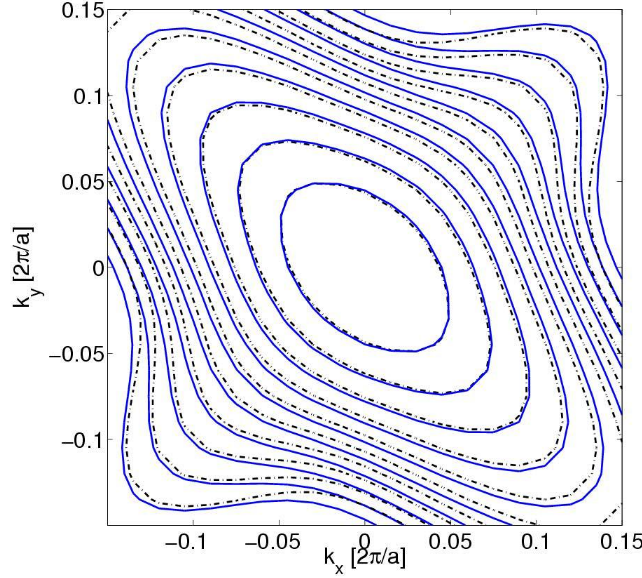

Fig. 6. Comparison between the EPM band structure calculations (solid lines) and the analytical model (7) (dashed lines) at the minimum $k_{\min}$ from (8) for shear strain ε_{xy} = 1%. The analytical model predicts the anisotropy of the transversal effective mass on shear strain. The contours are spaced at 50 meV.

$$H_{ii}(\mathbf{k}) = H_{ii}^{0}(\mathbf{k}) + \delta E, \qquad i = 1, 2$$

where $\delta E = \Xi_d(\varepsilon_{xx} + \varepsilon_{yy} + \varepsilon_{zz}) + \Xi_u \varepsilon_{zz}$ with Ξ_d denoting the dilation and Ξ_u the uniaxial deformation potentials for the conduction band. The off-diagonal elements of the Hamiltonian are [7]:

$$H_{12}(\mathbf{k}) = \frac{\hbar^2 k_x k_y}{M} - D\varepsilon_{xy}\,, \tag{6}$$

where D = 14 eV denotes the shear deformation potential.

The dispersion relation of the [001] valleys including the shear strain component for the conduction band now reads:

$$E(\mathbf{k}) = \frac{\hbar^2 k_z^2}{2m_l} + \frac{\hbar^2(k_x^2 + k_y^2)}{2m_t} + \delta E - \sqrt{\left(\frac{k_z p}{m_0}\right)^2 + \left(\frac{\hbar^2 k_x k_y}{M} - D\varepsilon_{xy}\right)^2}\,. \tag{7}$$

Because of shear strain the minimum $k_{\min}$ moves closer to the X point. From (7) we obtain

$$k_{\min} = k_0\sqrt{1-\eta^2}, \qquad |\eta| < 1\,, \tag{8a}$$

$$k_{\min} = 0, \qquad |\eta| > 1. \tag{8b}$$

Here, the dimensionless off-diagonal strain $\eta = 2D\varepsilon_{xy}/\Delta$ is introduced. Interestingly, for $\eta \geq 1$ the valley minimum is exactly at the X point. The minimum also moves down in energy by $\Delta E_{\min}$ with respect to the remaining degenerate valleys. For $|\eta| \leq 1$ the strain dependence is quadratic:

$$\Delta E_{\min} = -\eta^2 \Delta / 4\,, \qquad |\eta| \leq 1\,; \tag{9a}$$

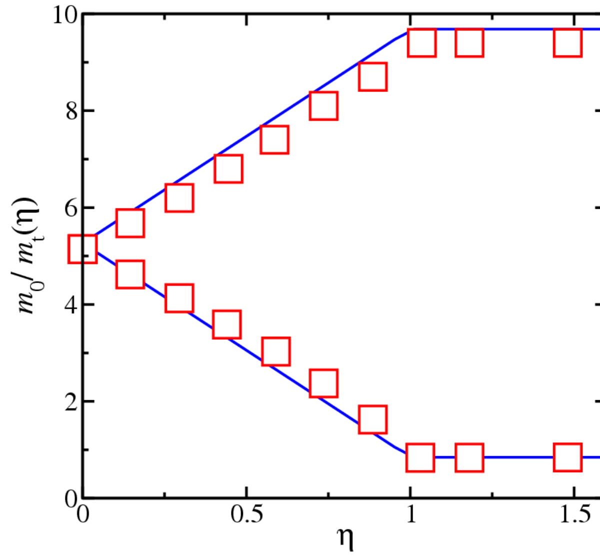

Fig. 7. Comparison of (10) and transversal masses extracted from EPM band structure calculations. The lower branch corresponds to m_t^- and the upper to m_t^+. Excellent agreement between numerical results and the analytical expressions (10) is found.

while it is linear for $|\eta| \geq 1$:

$$\Delta E_{\min} = -(2|\eta|-1)\Delta/4, \qquad |\eta| \geq 1. \tag{9b}$$

In Fig.6 we compare the results of the EPM calculations with the analytical model (5) at the minimum $k_{\min}$ for $\varepsilon_{xy} = 1\%$. The agreement between the two-band **k·p** model and the EPM calculations is excellent. In contrast to the unstrained case shown in Fig.4 the dispersion relation at small k_x and k_y becomes anisotropic displaying the dependence of the transversal effective mass on shear strain. Evaluating the second derivatives of (7) at the band minimum (8), we obtain two different branches for the inverse effective mass across (-) and along (+) the tensile stress in [110] direction:

$$m_t / m_t^{\mp}(\eta) = \left[1 \pm \eta\, m_t / M\right], \qquad |\eta| \leq 1; \tag{10a}$$

$$m_t / m_t^{\mp}(\eta) = \left[1 \pm m_t / M\right], \qquad |\eta| \geq 1, \tag{10b}$$

Good agreement between the inverse transversal effective masses evaluated numerically by EPM and found from (10) is demonstrated in Fig.8.
(7) also allows evaluation of the dependence of the longitudinal mass $m_l(\eta)$ on strain. The longitudinal mass $m_l(\eta)$ can be written as:

$$m_l(\eta) / m_l = \left[1 - \eta^2\right]^{-1}, \qquad |\eta| \leq 1; \tag{11a}$$

$$m_l(\eta) / m_l = \left[1 - |\eta|^{-1}\right]^{-1}, \qquad |\eta| \geq 1. \tag{11b}$$

5. CONCLUSION

Predictions of the two-band **k·p** model are compared with the results of the empirical nonlocal pseudo-potential method and the *sp³d⁵s** nearest-neighbor tight-binding model. It is demonstrated that the two-band **k·p** model is consistent with the results of the empirical pseudo-potential method. The model accurately describes the whole band structure around the valley minimum, including the effective masses and the band non-parabolicity. It is shown that the $sp^3d^5s^*$ model overestimates the gap between the two lowest conduction bands at the valley minimum and consequently underestimates the anisotropy due to non-parabolic effects. The two-band **k·p** model allows to account for shear strain, which leads to profound changes in the conduction band causing the valley minima to shift and the effective masses to change. Predictions of the two-band **k·p** method are in good agreement with the results of the pseudo-potential method.

ACKNOWLEDGEMENT

This work was supported by the Austrian Science Fund FWF, project P19997-N14.

REFERENCES

[1] J.M. Luttinger and W. Kohn, "Motion of Electrons and Holes in Perturbed Periodic Fields", *Phys.Rev*. **97**, 869—883 (1955).

[2] K. Uchida, A. Kinoshita, and M. Saitoh, "Carrier Transport in (110) nMOSFETs: Subband Structure, Non-Parabolicity, Mobility Characteristics, and Uniaxial Stress Engineering", in *IEDM Techn. Dig*. (2006), pp. 1019—1021.

[3] K. Uchida, T. Krishnamohan, K.C. Saraswat, and Y. Nishi, "Physical Mechanisms of Electron Mobility Enhancement in Uniaxial Stressed MOSFETs and Impact of Uniaxial Stress Engineering in Ballistic Regime", in *IEDM Techn. Dig*. (2005), pp.129—132.

[4] E. Ungersboeck, V. Sverdlov, H. Kosina, and S. Selberherr, "Electron Inversion Layer Mobility Enhancement by Uniaxial Stress on (001) and (100) Oriented MOSFETs, in *Proc. Intl. Conf. on Simulation of Semiconductor Processes and Devices* (2006), pp. 43—46.

[5] E. Ungersboeck, S. Dhar, G. Karlowatz, V. Sverdlov, H. Kosina, and S. Selberherr, "The Effect of General Strain on Band Structure and Electron Mobility of Silicon", *IEEE Trans.Electron Devices* **54**, 2183—2190 (2007).

[6] V. Sverdlov, E. Ungersboeck, H. Kosina, and S. Selberherr, "Influence of Uniaxial [110] Stress on Silicon Band Structure and Electron Low-Field Mobility in Ultra-Thin Body SOI FETs", in *Proc. EUROSOI* 2007 (2007), pp.39—40.

[7] J.C. Hensel, H. Hasegawa, and M. Nakayama, "Cyclotron Resonance in Uniaxially Stressed Silicon. II. Nature of the Covalent Bond", *Phys.Rev*. **138**, A225—A238 (1965).

[8] D. Rideau, M. Feraille, L. Ciampolini, M. Minondo, C. Tavernier, H. Jaouen, A. Ghetti, "Strained Si, Ge, and $Si_{1-x}Ge_x$ Alloys Modeled with a First-Principles-Optimized Full-Zone **kp** Method", *Phys.Rev. B* **74**, 195208-1—20 (2006).

[9] M.M. Rieger and P. Vogl, "Electronic-Band Parameters in Strained $Si_{1-x}Ge_x$ Alloys on $Si_{1-y}Ge_y$ Substrates", *Phys.Rev. B* **48**, 14276—14287 (1993).

[10] T.B. Boykin, G. Klimeck, and F. Oyafuso, "Valence Band Effective-Mass Expressions in the $sp^3d^5s^*$ Empirical Tight-Binding Model Applied to a Si and Ge Parametrization", *Phys.Rev. B* **69**, 115201-1—10 (2004).

[11] C. Jacoboni and L. Reggiani, "The Monte Carlo Method for the Solution of Charge Transport in Semiconductors with Applications to Covalent Materials", *Rev.Mod.Phys*. **55**, 645—705 (1983).

[12] I. Balslev, "Influence of Uniaxial Stress on the Indirect Absorption Edge in Silicon and Germanium", *Phys.Rev*. **143**, 636—647 (1966).